2020-08

Superior High-Energy-Density Biocidal Agent Achieved with a 3D MetalOrganic Framework

Zhang, Jichuan; Zhu, Zhenya; Zhou, Mingquing; Zhang, Jiaheng; Hooper, Joseph P.; Shreeve, Jean'ne

ACS Publications

Zhang, Jichuan, et al. "Superior High-Energy-Density Biocidal Agent Achieved with a 3D MetalOrganic Framework." ACS Applied Materials & Interfaces 12.36 (2020): 40541-40547.
http://hdl.handle.net/10945/69318

ACS APPLIED MATERIALS & INTERFACES

www.acsami.org

Research Article

Superior High-Energy-Density Biocidal Agent Achieved with a 3D Metal–Organic Framework

Jichuan Zhang, Zhenye Zhu, Mingqing Zhou, Jiaheng Zhang,* Joseph P. Hooper, and Jean'ne M. Shreeve*

Cite This: *ACS Appl. Mater. Interfaces* 2020, 12, 40541–40547

Read Online

ACCESS | Metrics & More | Article Recommendations | Supporting Information

ABSTRACT: A significant number of challenges are encountered when developing biocidal agents with high throwing capacity for biosafety applications. Now a three-dimensional metal–organic framework (3D MOF) {**MOF (2)**, $[Cu(atrz)(IO_3)_2]_n$ (atrz = 4,4′-azo-1,2,4-triazole)} was obtained using a postsynthetic method from **MOF (1)** {$[Cu(atrz)_3(NO_3)_2]_n$}. Benefitting from the oxygen-rich and small volume of the iodate (IO_3) ligands (2.73 Å) in **MOF (2)** compared to the atrz ligand (7.70 Å) in **MOF (1)**, the density of **MOF (2)** is 3.168 g cm^{-3}, nearly twice that of its precursor. Its detonation velocity of 7271 ms^{-1} exceeds that of TNT (trinitrotoluene) and its detonation pressure of 40.6 GPa is superior to that of HMX (cyclotetramethylenetetranitramine) (1,3,5,7-tetranitro-1,3,5,7-tetrazoctane, 39.2 Gpa), which are the highest detonation properties for a biocidal agent. Its superior detonation performance results in its main product, I_2, being distributed over a wide area, markedly reducing the diffusion of harmful microorganisms. This study offers novel insight not only for high-energy-density materials but also for huge potential applications as biocidal agents.

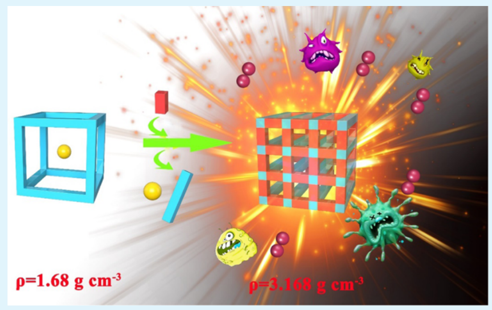

KEYWORDS: *3D metal–organic framework, biocidal agent, energetic materials, high energy density, iodine*

INTRODUCTION

Development in modern science and technology has allowed people to live in environments with increased biosafety relative to the previous century. Frequent occurrences of biocrises cause widespread disasters for people, animals, and the environment.[1,2] These crises result from various reasons including the use of bioweapons by extremists, leakage of bioagents from storage, and outbreaks of organisms and toxins (such as SARS, Ebola, H7N9, and African Swine fever).[3−8] For example, in 2001, a series of letters containing anthrax spores were sent by mail in the USA. In the process, 22 people were seriously injured, five of whom died, and probably thousands were contaminated and advised to use antibiotics for an extended period of time.[9] At the beginning of 2020, the outbreak of COVID-19 has caused many deaths all over the world.[10] The growth in the number of biocrises has led to an increase in the scope and magnitude of highly infectious diseases.[11,12] Traditional biocidal methods require a significant effort to distribute antibiological agents. However, this tends to be inefficient, susceptible to infection for people, and cannot be distributed over a large range, especially in those places that are difficult to reach. Preventing the diffusion of these harmful microorganisms and improving their rapid elimination on a large scale is an enormous challenge.

Iodine is an efficient biocidal agent for bacteria, fungi, yeasts, viruses, spores, and protozoan parasites (a 99.999% kill in 10 min at 25 °C).[13] However, since it sublimes readily, elemental iodine itself is not useful as an antibiological agent. Until recently, the emergence of iodine-containing energetic compounds, which can kill harmful microorganisms by releasing I_2 upon initiation, was a milestone for both energetic materials and antibiological agents.[14−27] These compounds not only improved the biocidal efficiency but also precluded the sublimation of iodine in the antibiological agents. Nevertheless, the drawbacks of the current iodine-containing energetic agents are notable. (1) The detonation performances of all of the reported iodine-containing compounds are low {only one compound, 3,3,3-trinitropropyl-1-ammonium periodate is higher than that of TNT (2,4,6-trinitrotoluene)}, while its iodine content is only 32.9%, and its decomposition temperature is only 138 °C,[27] which is unsuitable for a biocidal agent. (2) The energy level of most iodine-containing compounds is too low to allow ignition, and the mixture of iodine-containing agents with explosives complicates the process of energetic iodine-containing agents and may likely result in accidents. (3) Nearly all of the iodine-containing agents are obtained through organic syntheses that result from costly multistep reactions

Received: July 6, 2020
Accepted: August 13, 2020
Published: August 13, 2020

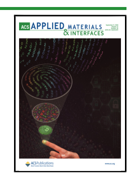

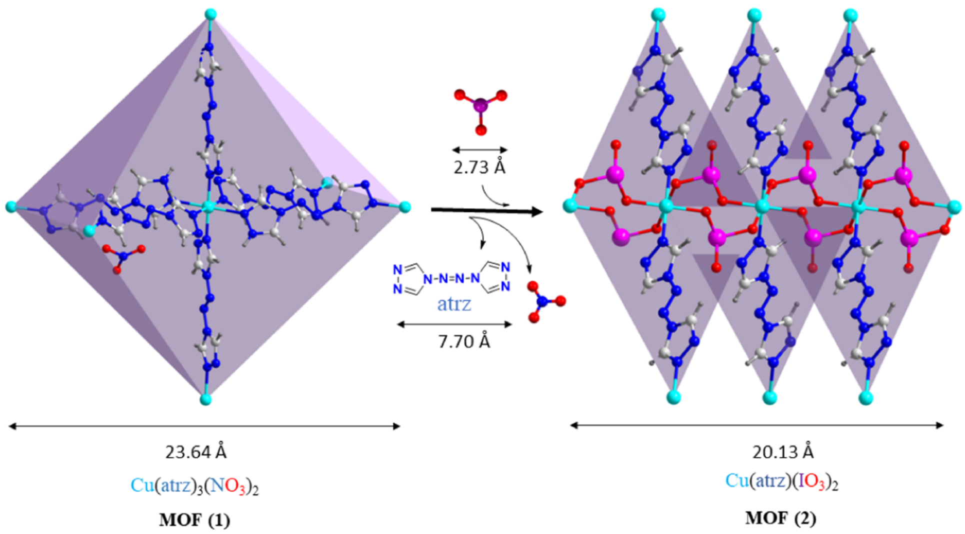

Figure 1. Change in the crystal sizes of **MOF (1)** and **MOF (2)**.

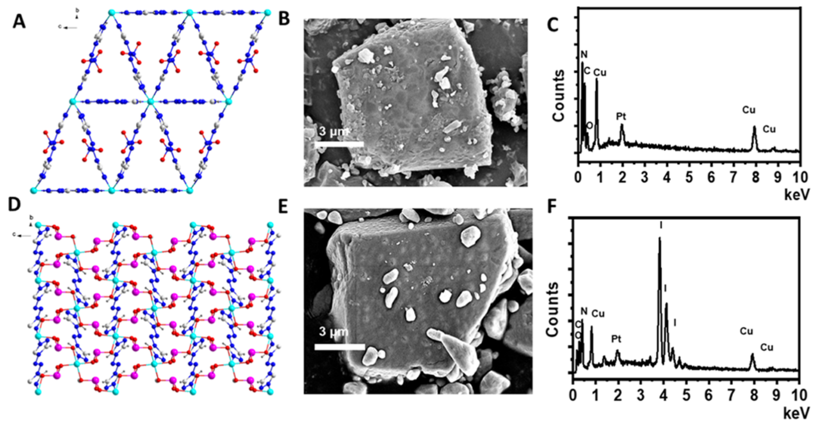

Figure 2. (A, D) Packing structure of **MOF (1)** and **MOF (2)** viewed from a-axis, respectively. (B, E) SEM (scanning electron microscopy) images of **MOF (1)** and **MOF (2)**, respectively. (C, F) EDX (energy-dispersive X-ray spectroscopy) scans of **MOF (1)** and **MOF (2)**, respectively.

and produce organic waste that is not environmentally friendly. Therefore, developing novel iodine-containing agents that exhibit superior detonation properties by a simple method is worthwhile as well as being significantly challenging.

Three-dimensional metal−organic frameworks (3D MOFs) have been utilized extensively in catalysts, drug transportation, absorption, and separation since the beginning of the 21st century due to their excellent porosity.[28,29] Energetic 3D MOFs are a unique type of 3D MOFs that are comprised of energetic nitrogen-rich ligands and metal ions.[30−32] Energetic 3D MOFs have drawn significant attention since the first report of **MOF (1)**, $[Cu(atrz)_3(NO_3)_2]_n$ (atrz = 4,4′-azo-1,2,4-triazole), because of its high thermal stability and low sensitivity.[33] Just as with traditional energetic materials, the primary aim of energetic 3D MOFs is to achieve high energy density (minimum porosity). However, their detonation properties and densities still have not been realized because (1) the presence of two or three ligands in the unit cell leads to a low oxygen balance in the energetic 3D MOFs, even with oxygen-rich anions (NO_3, ClO_4), and (2) the empty volumes of most energetic 3D MOFs are higher than those of organic compounds, leading to an energetic density even lower than that of the organic compounds. For example, the oxygen balance of **MOF (1)** is −58.82%, and the length of atrz is 7.70 Å, resulting in the density of **MOF (1)** to be only 1.64 g cm^{-3}, which is even lower than those of most organic energetic compounds (Figure S1). Although several strategies have been employed including introducing more energetic molecules or anions in the holes of 3D MOFs or replacing ligands with smaller-volume nitrogen-rich ligands to increase the energetic densities of 3D MOFs, the desired results are still elusive.[34−37] Hence, employing a novel strategy to change this situation is necessary.

Recently, a postsynthetic method has become increasingly interesting for preparing MOFs because the conditions employed are mild, which facilitates the investigation of their synthesis mechanisms.[38] In addition, the IO_3^- anion serves both roles of being iodine and oxygen rich. Due to the larger atomic radius and lower electronegativity of iodine relative to fluorine and chlorine anions, the coordination ability of the IO_3^- anion is strong.[39,40] Thus, if the IO_3^- anion replaces one or two nitrogen-rich ligands in an energetic 3D MOF, the oxygen balance, density, and energy level of the new MOF will be increased greatly, and the new MOF will exhibit a biocidal effect upon decomposition. Now KIO_3 was chosen to exchange with **MOF (1)**, and the properties including crystal structure, energetic performance, and biocidal effect of the resulting MOF were studied extensively.

https://dx.doi.org/10.1021/acsami.0c12251
ACS Appl. Mater. Interfaces 2020, 12, 40541−40547

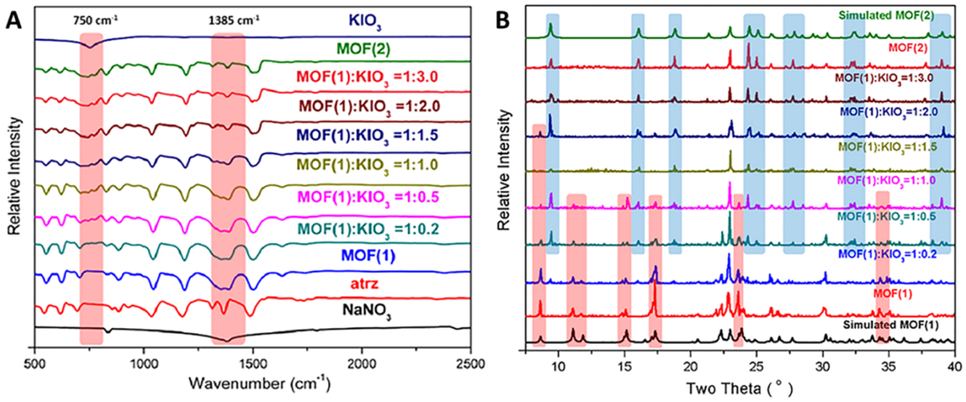

Figure 3. Transformations of FT-IR (A) and XRD (B) during postsynthesis.

RESULTS AND DISCUSSION

Synthesis and Single-Crystal Structure. **MOF (1)** was immersed in a solution of KIO_3 (2.1 M) for 24 h at room temperature. The color of the crystals changed from blue to baby blue (S2, Supporting information). The resulting crystal structure was determined by X-ray diffraction to be monoclinic (*P*21/*c*), with one Cu, one atrz ligand, and two IO_3^- anions in each unit cell of **MOF (2)** $[Cu(atrz)(IO_3)_2]_n$. Two atrz ligands that play the role of a counterion in **MOF (1)** were replaced by IO_3^- anions for the same role. The coordination of Cu in **MOF (2)** approaches a regular octahedron and is similar to that found in **MOF (1)**. Due to the diameter of IO_3^- (2.73 Å), which is less than that of atrz, the lengths of the two diagonals of the rectangle in **MOF (2)** were found to be only 20.13 Å, which is still shorter than that of a single diagonal in **MOF (1)** (Figure 1). In addition, the lengths of Cu−N and Cu−O bonds of **2** are 1.997, 1.994, and 2.318 Å, respectively, which are shorter than the three Cu−N bonds (2.009, 2.030, and 2.381 Å, respectively) in **MOF (1)**, correspondingly. The shorter Cu−N/O coordination bonds and IO_3 ligands in **MOF (2)** relative to **MOF (1)** give rise to a void volume (inverse with packing index) of **MOF (2)** as low as 22.3% (packing index 77.7%; Figure S1a). The closer packing of **MOF (2)** compared to **MOF (1)** is seen from Figure 2A,D. Meanwhile, the characterizations of scanning electron microscopy (SEM) and energy-dispersive X-ray (EDX) (Figures 2B,C,E,F and S3) show distinct differences between **MOF (1)** and **MOF (2)**. The **MOF (2)** is the second-lowest void volume based on 485 3D MOFs of transition metals, and it is just slightly higher than that of the lowest one (22.0%, $[CuBT(H_2O)]_n$, BT = 5,5′-bistetrazolate).[41] The packing index of **MOF (2)** is not only higher than that of **MOF (1)** (68.7%) but also higher than that of the majority of the energetic organic compounds (Figure S1b). The density of **MOF (2)** is 3.168 g cm^{-3}, which is almost twice that of its precursor (1.68 g cm^{-3}, 173 K).

To study the process and mechanism of exchange, **MOF (1)** was added to solutions that contained 0.2/0.5/1.0/1.5/2.0/3.0 M of KIO_3 at room temperature, respectively (S2). The resulting samples changed gradually from blue to baby blue over 24 h. After filtering and drying, these samples were characterized by FT-IR (Fourier transform infrared spectroscopy) (Figure 3A), XRD (X-ray diffraction) (Figure 3B). In FT-IR spectra, the characteristic peak of the NO_3^- anion is at ∼1385 cm^{-1} and that of the IO_3^- anion is at ∼750 cm^{-1}. With a gradual increase in the proportion of KIO_3, the NO_3^- anions of **MOF (1)** were gradually replaced by IO_3^-. This led to a decrease in the intensity of NO_3^- in these samples and an enhanced intensity of IO_3^-. Similarly, when the molar ratios between KIO_3 and **MOF (1)** increased gradually, the XRD characteristic peaks (2θ°: 8.6, 11.1, 11.7, 15.1, 17.3, 22.0, 22.6, 23.6, 26.2, 30.1, 33.9) of **MOF (1)** got increasingly weaker, while the characteristic peaks of **MOF (2)** (2θ°: 9.5, 16.1, 18.8, 21.3, 23.0, 24.4, 25.0, 27.8, 32.4, 37.8, 39.0) were found to get stronger. Finally, the combination of elemental analysis, FT-IR, and XRD tests shows that when the molar ratio between KIO_3 and **MOF (1)** is 2:1, crystalline **MOF (1)** was nearly converted completely into **MOF (2)**. When this ratio was increased to 3:1, **MOF (1)** was 100% changed into **MOF (2)**, which is supported by elemental analysis. Calculations based on NBO charge distribution and coordination bond energy (S4 and S5) were conducted to investigate the driving force of the exchange. The calculated results show that the charge density of the O atom (IO_3^-) was −1.227, which is considerably higher than that of NO_3^- (−0.561), suggesting that the possibility of the formation of a coordination bond between IO_3^- and Cu is markedly higher than that between Cu and NO_3^-. The calculated energies of the three Cu−N bonds in **MOF (1)** are 406.2, 409.5, and 254.0 kJ mol^{-1}, which are much lower than the two Cu−O bonds (673.1 and 654.1 kJ mol^{-1}) and the one Cu−N (614.9kJ mol^{-1}) bond of MOF (2). These results show that exchange between **MOF (1)** and KIO_3 occurs readily and that IO_3^- enhances the stability of **MOF (2)** relative to that of **MOF (1)**. The structure of **MOF (2)** is strengthened greatly, which is also supported by HPLC (high-performance liquid chromatography) tests. The HPLC tests of solubility show that **MOF (1)** is ∼17 times (7.06 g L^{-1}) more soluble in water than **MOF (2)** (S6). The solubility of **MOF (2)** was calculated to be 0.42 g L^{-1}, showing that it is slightly soluble in water. Given the above results of calculations and HPLC tests, **MOF (2)** could be synthesized from hot water (80 °C) in 30 s on a large scale using atrz, $Cu(NO_3)_2$, and KIO_3 in a molar ratio 1:1:2 (S7).

Physicochemical Properties. Excellent thermal stability and acceptable sensitivity values are basic requirements for promising energetic materials as well as biocidal agents. The decomposition temperature (onset) of **MOF (2)** is 267 °C measured at a nitrogen flow rate of 5 °C min^{-1} using a differential scanning calorimeter (DSC Q2000, S8). This value is not only higher than those of all of the IO_3^--containing organic compounds (their thermal stabilities are ≤190 °C)[24] but also higher than that of the classic explosive RDX (cyclotrimethylenetrinitramine, T_d = 210 °C), and it is

https://dx.doi.org/10.1021/acsami.0c12251
ACS Appl. Mater. Interfaces 2020, 12, 40541−40547

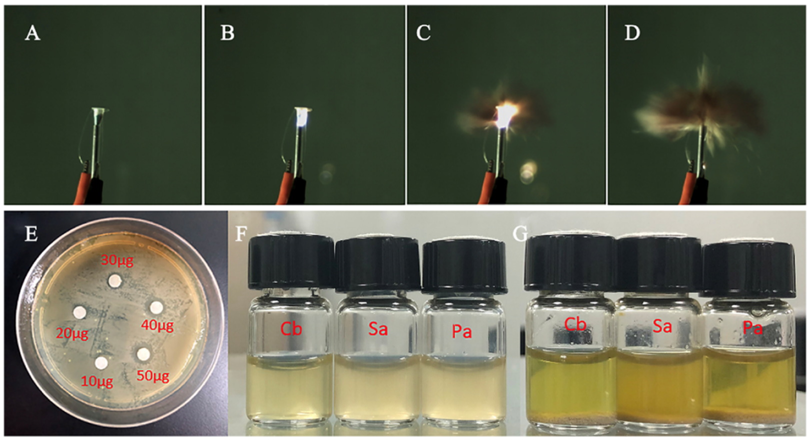

Figure 4. (A−D) Images of the explosion initiation captured by a high-speed camera with an interval of 0.2 ms. (E) Bactericide effect on *E. coli.* (F) Suspension solutions of three breeding bacteria. (G) Addition of the explosion products of **MOF (2)** into three breeding bacteria solutions in 30 min (dead bacteria: precipitate on the bottom of the culturing bottles).

comparable with HMX (cyclotetramethylenetetranitramine, T_d = 280 °C). Sensitivities to impact and friction were determined based on the BAM Standard,[42,43] which gave impact and friction sensitivities of **MOF (2)** of 18 J and 60 N (S9), respectively. These are considerably less sensitive than most reported IO_3^- examples. Higher thermal stability and lower sensitivity than those of IO_3^--based organic compounds should arise from the strong coordination bonds in **MOF (2)**. It should be noted that IO_3^- increases the oxygen balance of **MOF (2)** to −12.47% from −57.65% for **MOF (1)**. This is also higher than that of TNT (−74.00%), RDX (−21.62%), and HMX (−21.62%). The increased oxygen balance is very helpful in improving the detonation performance.

The heat of combustion of **MOF (2)** was determined to be 3469 kJ mol^{-1} with an Oxygen Bomb Calorimeter (PARR 1341EB, BOMB CALORI PLAIN). Its heat of formation was calculated to be 1181 kJ mol^{-1} using Hess's law (S9), which arises from the high heat of formation of the nitrogen-rich ligand[44] and the strong coordination bonds. With an experimental density of 3.11 g cm^{-3} at room temperature and heat of formation in hand, the detonation velocity of **MOF (2)** was calculated by Cheetah 8.0 to be 7271 ms^{-1}, which is the highest detonation velocity among all reported iodine-containing compounds and superior to that of TNT (6881 m^{-1}), and its detonation pressure is 40.61 Gpa, exceeding that of HMX (39.50 Gpa). This is higher than those of all reported detonation pressure values of iodine-containing compounds.[14−27] The surprisingly elevated detonation properties of **MOF (2)** are the result of an ideal combination of high heat of formation, high density, and excellent oxygen balance, which could disperse the explosion products over a larger area.

The iodine content of **MOF (2)** is 43.98%. When it was initiated, 43.17% I_2 would be released by **MOF (2)**, which was predicted by Cheetah 8.0 (S10 and Cheetah calculation file). This was observed as a purple cloud with a high-speed camera with an interval of 0.2 ms (Figure 4A−D). The iodine released plays the main role in the bactericidal effect, which was proved by biocidal tests in both solid and liquid phases. The small amount of Cu as well as CuO formed quickly after the explosion could also be useful as biocides.[45,46] The solid biocide tests were conducted according to previous work.[15] *Escherichia coli* (Ec), *Staphylococcus aureus* (Sa), and *Pseudomonas aeruginosa* (Pa) were chosen as representatives of harmful microorganisms because they are widely distributed on the earth and easily infect people.[47−49] The explosion products of **MOF (2)** were collected in an oxygen bomb with water and added to five circular papers (diameter = 3 mm) with varying amounts of decomposed samples of **MOF (2)** (10, 20, 30, 40, 50 μg portions, respectively). The circles were placed in the culture medium. The results showed that when the **MOF (2)** concentration was 30 μg, all bacteria were annihilated in 30 min (Figures 4E and S11). Based on the size of circles (28.26 mm^2), the effective biocidal quality of **MOF (2)** for 1 km^2 would be 1.06 ton. Given that the harmful microorganisms can also exist in water, the biocidal tests of these three bacteria were conducted in aqueous solutions. Products of **MOF (2)** were added into three vials, respectively, which contain these three breeding bacteria. Half an hour later, bacteria in each of the three vials were killed completely (Figure 4F,G), and the minimum biocidal concentrations responding to **MOF (2)** for these three bactericides are the same, at 3 mg mL^{-1}. Although the biocidal capacity of **MOF (2)** is slightly lower than that of DIDNPT (2,6-diiodo-3,5-dinitro-4,9-dihydrodipyrazolo [1,5-a:5′,1′-d][1,3,5]triazine), (Table S5),[15] which could kill bacteria over 1 km^2 with about 0.8 ton, the detonation performance of **MOF (2)** is considerably higher than that of DIDNPT and could distribute the products of **MOF (2)** to a larger area to kill much more harmful bacteria.

■ CONCLUSIONS

In summary, iodine-containing 3D **MOF (2)** was obtained by methods of exchange and synthesis, and the exchange process and mechanism were studied extensively. Distinct from the reported 3D MOFs, the short and strong coordination ability of IO_3^- anions play both the role of the ligand as well as a counterion. This results in (1) the oxygen balance of **MOF (2)** at −12.47%, which is higher than those of classic explosives such as TNT, RDX, and HMX and its precursor **MOF (1)**; (2) the density of **MOF (2)** is 3.168 g cm^{-3}, which is nearly twice relative to **MOF (1)**; and (3) high thermal stability and low sensitivity among iodate compounds. High density, high heat of formation, and a less negative oxygen balance give rise to a detonation velocity for **MOF (2)** of 7271 m s^{-1}, which is the highest detonation velocity found for iodine-containing compounds. Additionally, its detonation pressure is higher

https://dx.doi.org/10.1021/acsami.0c12251
ACS Appl. Mater. Interfaces 2020, 12, 40541−40547

than that of HMX. Superior detonation performance combined with excellent biocidal effects suggests that the explosion products including iodine (a biocide) could be distributed over a large area, which will prevent the diffusion of harmful microorganisms through annihilation. This study provides a novel inroad into high-energy-density materials and potentially valuable biocidal agents in infection control.

EXPERIMENTAL SECTION

Safety Precautions. Although none of the energetic MOFs described herein have exploded or detonated in the course of this research, these materials should be handled with extreme care using the best safety practices.

General Methods. **MOF (1)** was prepared according to the literature.[32] All other materials were commercially available and used without further purification. Powder X-ray diffraction (PXRD) patterns of the samples were analyzed with monochromatized Cu Kα (λ = 1.54178 Å) incident radiation by Bruker D8 Advance X-ray diffractometer operating at 40 kV voltage and 50 mA current. PXRD patterns were recorded from 5 to 80° (2θ) at 298 K. IR spectra were recorded using KBr pellets with a FT-IR spectrometer (Thermo Nicolet AVATAR 370). Density was determined at room temperature by employing a Micromeritics AccuPyc II 1340 gas pycnometer. Decomposition (onset) temperatures were recorded using a dry nitrogen gas purge and a heating rate of 5 °C min^{-1} on a differential scanning calorimeter (DSC, TA Instruments Q2000). Elemental analyses (C, H, N) were performed with a Vario Micro cube Elementar Analyser. Impact and friction sensitivity measurements were made using a standard BAM Fall hammer and a BAM friction tester.

X-ray Crystallography. Single blue block-shaped crystals of **MOF (2)** were used as received. A suitable crystal 0.12 × 0.12 × 0.08 mm^3 was selected and mounted on a nylon loop with paratone oil on a Bruker APEX-II CCD diffractometer. The crystal was kept at a steady temperature T = 173(2) K during data collection. The structure was solved with ShelXT[50] structure solution program using the Intrinsic Phasing solution method and using Olex2[51] as the graphical interface. The model was refined with version 2018/3 of ShelXL[52] using least-squares minimization.

ASSOCIATED CONTENT

Supporting Information

The Supporting Information is available free of charge at https://pubs.acs.org/doi/10.1021/acsami.0c12251.

Statistic works; exchange experiments and comparison of the single-crystal structures of **MOF (1)** and **MOF (2)**; characterizations of SEM and EDX; NBO calculations; energy calculations of coordination bonds; HPLC; synthesis of **MOF (2)**; thermal stability; physiochemical properties; determination of I content; and biocidal experiments and fluorescent staining (PDF)

Notional detonation/combustion properties (PDF)

Data was collected using a BRUKER CCD (charge coupled device) based diffractometer equipped with an Oxford low-temperature apparatus operating at 173 K (TXT)

AUTHOR INFORMATION

Corresponding Authors

Jiaheng Zhang − *Research Centre of Flexible Printed Electronic Technology, Harbin Institute of Technology, Shenzhen 518055, China; Zhuhai Institute of Advanced Technology Chinese Academy of Sciences, Biomaterials Research Center, Zhuhai 519003, China;* orcid.org/0000-0002-2377-9796; Email: zhangjiaheng@hit.edu.cn

Jean'ne M. Shreeve − *Department of Chemistry, University of Idaho, Moscow, Idaho 83844-2343, United States;* orcid.org/0000-0001-8622-4897; Email: jshreeve@uidaho.edu

Authors

Jichuan Zhang − *Department of Chemistry, University of Idaho, Moscow, Idaho 83844-2343, United States; Research Centre of Flexible Printed Electronic Technology, Harbin Institute of Technology, Shenzhen 518055, China; Zhuhai Institute of Advanced Technology Chinese Academy of Sciences, Biomaterials Research Center, Zhuhai 519003, China*

Zhenye Zhu − *Research Centre of Flexible Printed Electronic Technology, Harbin Institute of Technology, Shenzhen 518055, China;* orcid.org/0000-0001-9601-7963

Mingqing Zhou − *Research Centre of Flexible Printed Electronic Technology, Harbin Institute of Technology, Shenzhen 518055, China*

Joseph P. Hooper − *Department of Physics, Naval Postgraduate School, Monterey, California 93943, United States;* orcid.org/0000-0003-4899-1934

Complete contact information is available at: https://pubs.acs.org/10.1021/acsami.0c12251

Notes

The authors declare no competing financial interest.

ACKNOWLEDGMENTS

Financial support of the Office of Naval Research (N00014-16-1-2089) and the Defense Threat Reduction Agency (HDTRA 1-15-1-0028) is gratefully acknowledged. This work was supported by the National Natural Science Foundation of China (21905069), the Shenzhen Science and Technology Innovation Committee (JCYJ20180507183907224, KQTD20170809110344233), and Economic, Trade and Information Commission of Shenzhen Municipality through the Graphene Manufacture Innovation Center (201901161514).

REFERENCES

(1) Boddie, C.; Watson, M.; Ackerman, G.; Gronvall, G. K. Assessing the Bioweapons Threat. *Science* **2015**, *349*, 792−793.

(2) Berger, K. M. What Life Scientists Should Know about Security Threats. *Science* **2016**, *354*, 1237−1239.

(3) Seelos, C. Lessons from Iraq on Bioweapons. *Nature* **1999**, *398*, 187−188.

(4) Stenseth, N. C.; Atshabar, B. B.; Begon, M.; Belmain, S. R.; Bertherat, E.; Carniel, E.; Gage, K. L.; Leirs, H.; Rahalison, L. Plague: Past, Present, and Future. *PLoS Med.* **2008**, *5*, No. e3.

(5) Fouchier, R. A. M.; Kuiken, T.; Schutten, M.; Amerongen, G. V.; Doornum, G. J. J.; Hoogen, B. G. V.; Peiris, M.; Lim, W.; Stöhr, K.; Osterhaus, A. D. M. E. Koch's Postulates Fulfilled for SARS Virus. *Nature* **2003**, *423*, No. 240.

(6) Feldmann, H.; Geisbert, T. W. Ebola Haemorrhagic Fever. *Lancet* **2011**, *377*, 849−862.

(7) Costard, S.; Wieland, B.; Glanville, W. D.; Jori, F.; Rowlands, R.; Vosloo, W.; Roger, F.; Pfeiffer, D. U.; Dixon, L. K. African Swine Fever: How Can Global Spread be Prevented? *Philos. Trans. R. Soc., B* **2009**, *364*, 2683−2696.

(8) Riedel, S. Biological Warfare and Bioterrorism: a Historical Review. *Proc. (Bayl. Univ. Med. Cent.)* **2004**, *17*, 400−406.

(9) Jansen, H. J.; Breeveld, F. J.; Stijnis, C.; Grobusch, M. P. Biological Warfare, Bioterrorism, and Biocrime. *Clin. Microbiol. Infect.* **2014**, *20*, 488−496.

https://dx.doi.org/10.1021/acsami.0c12251
ACS Appl. Mater. Interfaces 2020, 12, 40541−40547

(10) Huang, C.; Wang, Y.; Li, X.; Ren, L.; Zhao, J.; Hu, Y.; Zhang, L.; Fan, g.; Xu, J.; Gu, X.; Cheng, Z.; Yu, T.; Xia, J.; Wei, Y.; Wu, W.; Xie, X.; Yin, W.; Li, H.; Liu, M.; Xiao, Y.; Gao, H.; Guo, L.; Xie, J.; Wang, G.; Jiang, R.; Gao, Z.; Jin, Q.; Wang, J.; Cao, B. Clinical Features of Patients Infected with 2019 Novel Coronavirus in Wuhan, China. *Lancet* **2020**, *395*, 497−506.

(11) https://www.ncbi.nlm.nih.gov/books/NBK493217/. Dec 8, 2012.

(12) Narayanan, N.; Lacy, C. R.; Cruz, J. E.; Nahass, M.; Karp, J.; Barone, J. A.; Hermes-DeSantis, E. R. Disaster Preparedness: Biological Threats and Treatment Options. *Pharmacol. Ther.* **2018**, *38*, 217−234.

(13) Kaiho, T. *Iodine Chemistry and Applications*; John Wiley & Sons, Inc.: New York, 2015.

(14) Agrawal, J. P.; Hodgson, R. D. *Organic Chemistry of Explosives*; John Wiley & Sons Ltd., Copyright 2007.

(15) Zhao, G.; He, C.; Zhou, W.; Hooper, J. P.; Imler, G. H.; Parrish, D. A.; Shreeve, J. M. Control of Biohazards: a High Performance Energetic Polycyclized Iodine-containing Biocide. *Inorg. Chem.* **2018**, *57*, 8673−8680.

(16) Chand, D.; He, C.; Hooper, J. P.; Mitchell, L. A.; Parrish, D. A.; Shreeve, J. M. Mono-and Diiodo-1, 2, 3-triazoles and Their Mono Nitro Derivatives. *Dalton Trans.* **2016**, *45*, 9684−9688.

(17) Chand, D.; Shreeve, J. M. Versatile Synthesis and Promise. *Chem. Commun.* **2015**, *51*, 3438−3441.

(18) Chand, D.; He, C.; Mitchell, L. A.; Parrish, D. A.; Shreeve, J. M. Electrophilic Iodination: a Gateway to High Iodine Compounds and Energetic Materials. *Dalton Trans.* **2016**, *45*, 13827−13833.

(19) Zhao, G.; He, C.; Kumar, D.; Hooper, J. P.; Imler, G. H.; Parrish, D. A.; Shreeve, J. M. 1, 3, 5-Triiodo-2, 4, 6-trinitrobenzene (TITNB) from Benzene: Balancing Performance and High Thermal Stability of Functional Energetic Materials. *Chem. Eng. J.* **2019**, *378*, No. 122119.

(20) Chinnam, A. K.; Shlomovich, A.; Shamis, O.; Petrutik, N.; Kumar, D.; Wang, K.; Komarala, E. P.; Tov, D. S.; Sućeska, M.; Yan, Q. L.; Gozin, M. Combustion of Energetic Iodine-rich Coordination Polymer−Engineering of New Biocidal Materials. *Chem. Eng. J.* **2018**, *350*, 1084−1091.

(21) Zhao, G.; He, C.; Kumar, D.; Hooper, J. P.; Imler, G. H.; Parrish, D. A.; Shreeve, J. M. Functional Energetic Biocides by Coupling of Energetic and Biocidal Polyiodo Building Blocks. *Chem. Eng. J.* **2019**, *368*, 244−251.

(22) Zhao, G.; Kumar, D.; He, C.; Hooper, J. P.; Imler, G. H.; Parrish, D. A.; Shreeve, J. M. New Generation Agent Defeat Weapons: Energetic N,N′-Ethylene-Bridged Polyiodoazoles. *Chem. Eur. J.* **2017**, *23*, 16753−16757.

(23) He, C.; Zhang, J.; Shreeve, J. M. Dense Iodine-Rich Compounds with Low Detonation Pressures as Biocidal Agents. *Chem. Eur. J.* **2013**, *19*, 7503−7509.

(24) He, C.; Hooper, J. P.; Shreeve, J. M. Iodine-rich Imidazolium Iodate and Periodate Salts: En Route to Single-based Biocidal Agents. *Inorg. Chem.* **2016**, *55*, 12844−12850.

(25) He, C.; Zhao, G.; Hooper, J. P.; Shreeve, J. M. Energy and Biocides Storage Compounds: Synthesis and Characterization of Energetic Bridged Bis(triiodoazoles). *Inorg. Chem.* **2017**, *56*, 13547−13552.

(26) He, C.; Parrish, D. A.; Shreeve, J. M. Alkyl Ammonium Cation Stabilized Biocidal Polyiodides with Adaptable High Density and Low Ppressure. *Chem. Eur. J.* **2014**, *20*, 6699−6706.

(27) Unger, C. C.; Klapötke, T. M.; Krumm, B. Unusual Energetic Periodate, Sulfate and Amino-bistetrazolate Salts of the Trinitropropylammonium Cation. *Z. Anorg. Allg. Chem.* **2020**, *646*, 2−4.

(28) Cook, T. R.; Zheng, Y.; Stang, P. J. Metal−organic Frameworks and Self-assembled Supramolecular Coordination Complexes: Comparing and Contrasting the Design, Synthesis, and Functionality of Metal−organic Materials. *Chem. Rev.* **2013**, *113*, 734−777.

(29) Lu, G.; Li, S.; Guo, Z.; Farha, O. K.; Hauser, B. G.; Qi, X.; Wang, Y.; Wang, X.; Han, S.; Liu, X.; DuChene, J. S.; Zhang, H.; Zhang, Q.; Chen, X.; Ma, J.; Loo, S. C. J.; Wei, W. D.; Yang, Y.; Hupp, J. T.; Huo, F. Imparting Functionality to a Metal−organic Framework Material by Controlled Nanoparticle Encapsulation. *Nat. Chem.* **2012**, *4*, 310−316.

(30) Zhang, J.; Shreeve, J. M. 3D Nitrogen-rich Metal−organic Frameworks: Opportunities for Safer Energetics. *Dalton Trans.* **2016**, *45*, 2363−2368.

(31) McDonald, K. A.; Seth, S.; Matzger, A. J. Coordination Polymers with High Energy Density: An Emerging Class of Explosives. *Cryst. Growth Des.* **2015**, *15*, 5963−5972.

(32) Chen, S.; Jin, Y.; Xia, H.; Wang, K.; Liu, Y.; Zhang, Q. Synthesis of Fused Tetrazolo[1,5-b]pyridazine-based Energetic Compounds. *Energ. Mater. Front.* **2020**, DOI: 10.1016/j.enmf.2020.05.001.

(33) Li, S.; Wang, Y.; Qi, C.; Zhao, X.; Zhang, J.; Zhang, S.; Pang, S. 3D Energetic Metal−Organic Frameworks: Synthesis and Properties of High Energy Materials. *Angew. Chem., Int. Ed.* **2013**, *52*, 14031−14035.

(34) Du, Y.; Su, H.; Fei, T.; Hu, B.; Zhang, J.; Li, S.; Pang, S.; Nie, F. Structure−Property Relationship in Energetic Cationic Metal−Organic Frameworks: New Insight for Design of Advanced Energetic Materials. *Cryst. Growth Des.* **2018**, *18*, 5896−5903.

(35) Zhang, J.; Du, Y.; Dong, K.; Su, H.; Zhang, S.; Li, S.; Pang, S. Taming Dinitramide Anions within an Energetic Metal−organic Framework: A New Strategy for Synthesis and Tunable Properties of High Energy Materials. *Chem. Mater.* **2016**, *28*, 1472−1480.

(36) Huang, Y. Q.; Zhao, X. Q.; Shi, W.; Liu, W. Y.; Chen, Z. L.; Cheng, P.; Liao, D. Z.; Yan, S. P. Anions-directed Metal-mediated Assemblies of Coordination Polymers Based on the Bis(4, 4′-bis-1, 2, 4-triazole) Ligand. *Cryst. Growth Des.* **2008**, *8*, 3652−3660.

(37) Ding, B.; Wang, Y. Y.; Liu, S. X.; Wu, X. X.; Zhu, Z. Z.; Huo, J. Z.; Liu, Y. Y. A Series of Multi-dimensional Metal−organic Frameworks with Trans-4, 4′-azo-1, 2, 4-triazole: Polymorphism, Guest Induced Single-crystal-to-single-crystal Transformation and Solvatochromism. *CrystEngComm* **2015**, *17*, 5396−5409.

(38) Cohen, S. M. Postsynthetic Methods for the Functionalization of Metal−organic Frameworks. *Chem. Rev.* **2012**, *112*, 970−1000.

(39) Li, G.; Shi, Z.; Liu, X.; Dai, Z.; Gao, L.; Feng, S. A New Inorganic− Organic Hybrid Copper Iodate with Potentially Large Void Volume. *Inorg. Chem* **2004**, *43*, 8224−8226.

(40) Sun, C. F.; Hu, C. L.; Xu, X.; Yang, B. P.; Mao, J. G. Explorations of New Second-order Nonlinear Optical Materials in the Potassium Vanadyl Iodate System. *J. Am. Chem. Soc.* **2011**, *133*, 5561−5572.

(41) Chen, S.; Zhang, B.; Yang, L.; Wang, L.; Zhang, T. Synthesis, Structure and Characterization of Neutral Coordination Polymers of 5, 5′-bistetrazole with Copper (II), Zinc (II) and Cadmium (II): A New Route to Reconcile Oxygen Balance and Nitrogen Content of High-energy MOFs. *Dalton Trans.* **2016**, *45*, 16779−16783.

(42) *Standardization Agreement 4489 (STANAG 4489), Explosives, Impact Sensitivity Tests*; NATO: Brussels, Belgium, 1999.

(43) *Standardization Agreement 4487 (STANAG 4487), Explosives, Friction Sensitivity Tests*; NATO: Brussels, Belgium, 2002.

(44) Xu, Y.; Wang, Q.; Shen, C.; Lin, Q.; Wang, P.; Lu, M. A Series of Energetic Metal Pentazolate Hydrates. *Nature* **2017**, *549*, 78−81.

(45) Khan, S. T.; Ahamed, M.; Al-Khedhairy, A.; Musarrat, J. Biocidal Effect of Copper and Zinc Oxide Nanoparticles on Human Oral Microbiome and Biofilm Formation. *Mater. Lett.* **2013**, *97*, 67−70.

(46) Ruparelia, J. P.; Chatterjee, A. K.; Duttagupta, S. P.; Mukherji, S. Strain Specificity in Antimicrobial Activity of Silver and Copper Nanoparticles. *Acta Biomater.* **2008**, *4*, 707−716.

(47) Moran, G. J.; Krishnadasan, A.; Gorwitz, R. J.; Fosheim, G. E.; McDougal, L. K.; Carey, R. B.; Talan, D. A. Methicillin-Resistant S. aureus Infections Among Patients in the Emergency Department. *N. Engl. J. Med.* **2006**, *355*, 666−674.

(48) Kaper, J. B.; Nataro, J. P.; Mobley, H. L. Pathogenic *Escherichia Coli*. *Nat. Rev. Microbiol.* **2004**, *2*, 123−140.

(49) Bodey, G. P.; Bolivar, R.; Fainstein, V.; Jadeja, L. Infections Caused by *Pseudomonas Aeruginosa*. *Rev. Infect. Dis.* **1983**, *5*, 279−313.

(50) Sheldrick, G. M. Crystal Structure Refinement with SHELXL. *Acta Crystallogr., Sect. C: Struct. Chem.* **2015**, *71*, 3−8.
(51) Dolomanov, O. V.; Bourhis, L. J.; Gildea, R. J.; Howard, J. A. K.; Puschmann, H. OLEX2: A Complete Structure Solution, Refinement and Analysis Program. *J. Appl. Crystallogr.* **2009**, *42* (2), 339−341.
(52) Sheldrick, G. M. *Acta Crystallogr., Sect. A: Found. Crystallogr.* **2008**, *64*, 112−122.

https://dx.doi.org/10.1021/acsami.0c12251
ACS Appl. Mater. Interfaces 2020, 12, 40541−40547